# Large electron mass anisotropy in a *d*-electron-based transparent conducting oxide: Nb-doped anatase $TiO_2$ epitaxial films

Yasushi Hirose,[1,2] Naoomi Yamada,[2] Shoichiro Nakao,[2] Taro Hitosugi,[2,3] Toshihiro Shimada,[1,2] and Tetsuya Hasegawa[1,2]
[1]*Department of Chemistry, The University of Tokyo, Tokyo 113-0033, Japan*
[2]*Kanagawa Academy of Science and Technology, Kawasaki 213-0012, Japan*
[3]*WPI-Advanced Institute for Materials Research, Tohoku University, Sendai 980-8577, Japan*
(Received 31 July 2008; revised manuscript received 13 September 2008; published 17 April 2009)

Electron mass anisotropy in the Nb-doped anatase $TiO_2$ (TNO) was determined by polarized infrared spectroscopy measurements for (012)-oriented TNO epitaxial films. The electron mass along the *c* axis, $m^*_{\langle 001\rangle}$, derived by Drude analyses, was found to be 0.5–3.3 $m_0$, which was 3–6 times larger than that along the *a* axis, $m^*_{\langle 100\rangle}$, 0.2–0.6 $m_0$. This large anisotropy was attributed to not only the anisotropic crystal structure but also the *d*-orbital-dominated conduction band. These results indicate that control of crystallographic orientation is of crucial importance for realizing high conductivity in polycrystalline TNO films.

DOI: 10.1103/PhysRevB.79.165108 PACS number(s): 73.61.−r

In the past decade, transparent conducting oxides (TCOs) have attracted much attention as indispensable materials for optoelectronic devices such as flat-panel displays, photovoltaic cells, and light emitting diodes.[1] Recently, we found that Nb-doped anatase $TiO_2$ (TNO) shows excellent conductivity ($\sigma > 1\times10^3\ \Omega^{-1}\ cm^{-1}$) and transparency for visible light (>75%) in the form of both epitaxial[2,3] and polycrystalline[4,5] film.

In contrast to other conventional TCOs with isotropic *s*-orbital-dominated conduction bands, such as Sn-doped $In_2O_3$ (ITO), Al-doped ZnO (AZO), and F-doped $SnO_2$ (FTO), the conduction band of TNO is mainly composed of anisotropic Ti 3*d* orbitals. This suggests that electrical transport in TNO is so anisotropic as to affect the conductivity of TNO polycrystalline films containing grains with different crystallographic orientation. Furubayashi *et al.*[3] determined electron mass $m^*$ along the *a* axis, $m^*_{\langle 100\rangle}$, to be 0.3–0.5 $m_0$ from optical measurements of the *c*-axis oriented TNO films. On the other hand, thermoelectric measurements revealed the density of state electron mass, $m^*_{DOS}$, which is a directional average of $m^*$, to be 0.3–1 $m_0$,[6,7] suggesting that $m^*$ along the *c* axis, $m^*_{\langle 001\rangle}$, is larger than $m^*_{\langle 100\rangle}$. However, a direct measurement of mass anisotropy on TNO has not yet been attempted, mainly because of the difficulty in growing bulk single crystals and epitaxial films with an orientation other than (001).

Here, we report on electron mass anisotropy, as determined by Drude analysis of polarized infrared (PIR) spectra of (012)-oriented TNO epitaxial films. The $m^*_{\langle 100\rangle}$ values obtained were 0.2–0.6 $m_0$, which are equivalent to those of conventional *s*-electron based TCOs, while $m^*_{\langle 001\rangle}$ was found to be 3–6 times larger than $m^*_{\langle 100\rangle}$. The origin of mass anisotropy will be discussed in terms of Ti 3*d* nature of the TNO conduction band.

Epitaxial $Ti_{1-x}Nb_xO_2$ ($x$=0, 0.002, 0.01, 0.03, and 0.06) films with (012) orientation were grown on $LaAlO_3$ (LAO) (011) single-crystalline substrates by pulsed laser deposition (PLD). A Kr:F excimer laser (248 nm, 2 J $cm^{-2}$, 2 Hz) was used for ablating sintered pellet targets composed of $TiO_2$ and $Nb_2O_5$. The deposition rate was ~0.1 Å $pulse^{-1}$, and the typical film thickness *d* was ~500 nm. The substrate temperature and oxygen partial pressure ($P_{O2}$) were set to 600 °C and $1\times10^{-5}$ Torr, respectively. The initial stage of the deposition (~3 nm thickness) was conducted at a $P_{O2}$ of $1\times10^{-3}$ Torr to prevent the growth of the rutile phase.[8]

Figure 1(a) is a typical $\theta$-$2\theta$ x-ray diffraction (XRD) pattern of the $Ti_{1-x}Nb_xO_2$ film grown on LAO (011) substrate, clearly indicating (024) diffraction peak of anatase

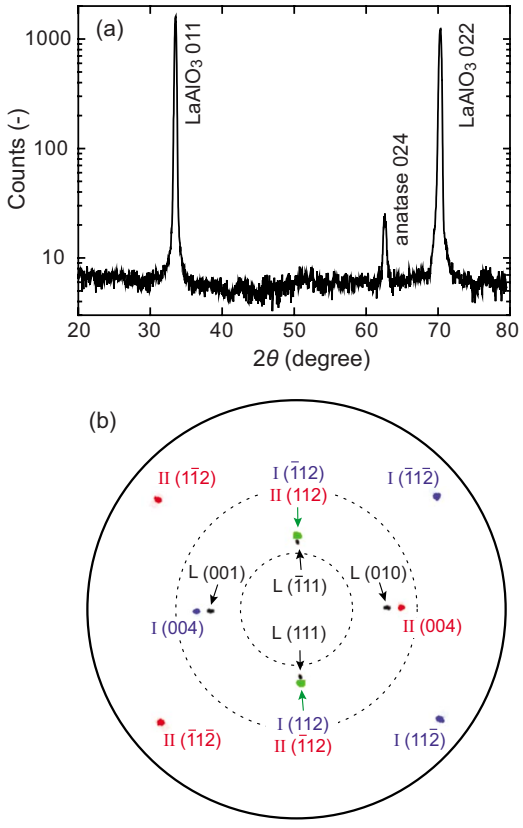


FIG. 1. (Color online) (a) $\theta-2\theta$ XRD pattern of a typical (012)-oriented TNO film grown on LAO (011) substrate. (b) Pole figure of the diffractions from anatase {004} and {112} planes (labeled with I or II) and LAO {100} and {111} planes (labeled with L). The labels I and II, respectively, indicate the epitaxial domains shown in Fig. 2. Dotted lines represent the tilt angles of 30° and 60°.

 

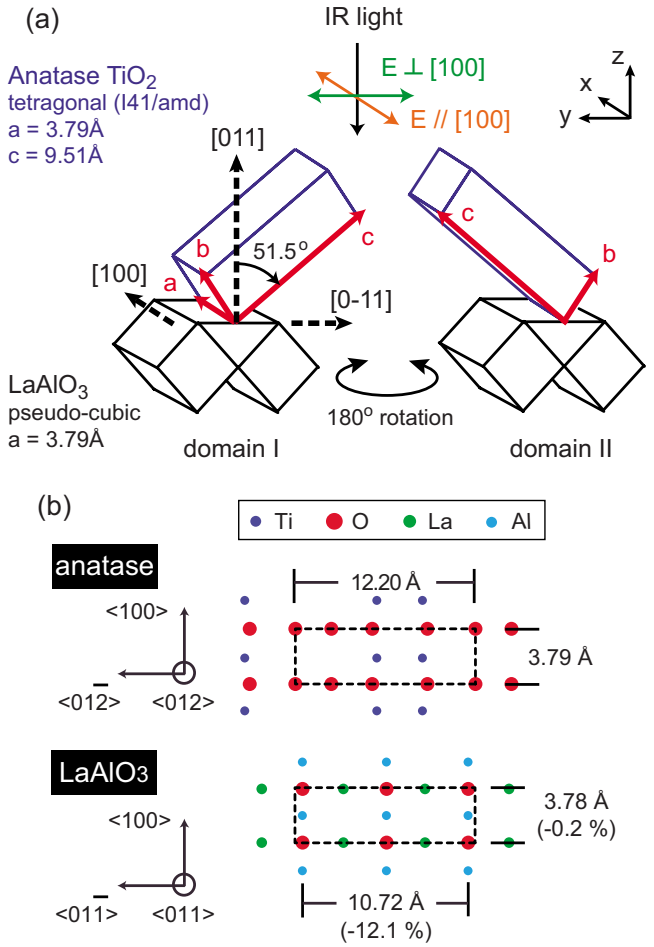


FIG. 2. (Color online) (a) Schematic of two epitaxial domains for TNO (012) film on LAO (011) substrate. Dashed arrows indicate the crystallographic directions of the LAO substrate. Configuration of the polarized IR measurements in experimental coordinate is also shown. (b) The models of atomic arrangements for anatase $TiO_2$ (012) and $LaAlO_3$ (011) surfaces.

$TiO_2$ without any secondary phases, such as rutile $TiO_2$, $Ti_nO_{2n-1}$, and $Nb_2O_5$. Pole figure measurements [Fig. 1(b)] exhibited that the TNO films consist of two equivalent epitaxial domains with 180° different in-plane orientations [Figs. 2(a) and 2(b)], being consistent with the previous reports on undoped anatase $TiO_2$.[9,10] The multidomain structure was also confirmed by cross-sectional transmission electron microscopy (TEM).[8] The domain size was evaluated as ~50–200 nm by atomic force microscopy and TEM measurements.

PIR reflection and transmission spectra were measured by an FT-IR spectrometer (PerkinElmer, Spectrum100) with a grid polarizer (Shimadzu, GPR-8000). The samples were irradiated with IR light at an incident angle of 0°, where the electric polarization vector **E** was either parallel ($\mathbf{E}_\parallel$) or perpendicular ($\mathbf{E}_\perp$) to the [100] direction of the TNO films, as illustrated in Fig. 2(a). PIR spectra of (001)-oriented TNO films grown on LAO (001) were also measured as reference. All PIR measurements were performed at room temperature.

Figure 3 shows PIR spectra measured for TNO films with different Nb concentrations. The undoped anatase $TiO_2$ film

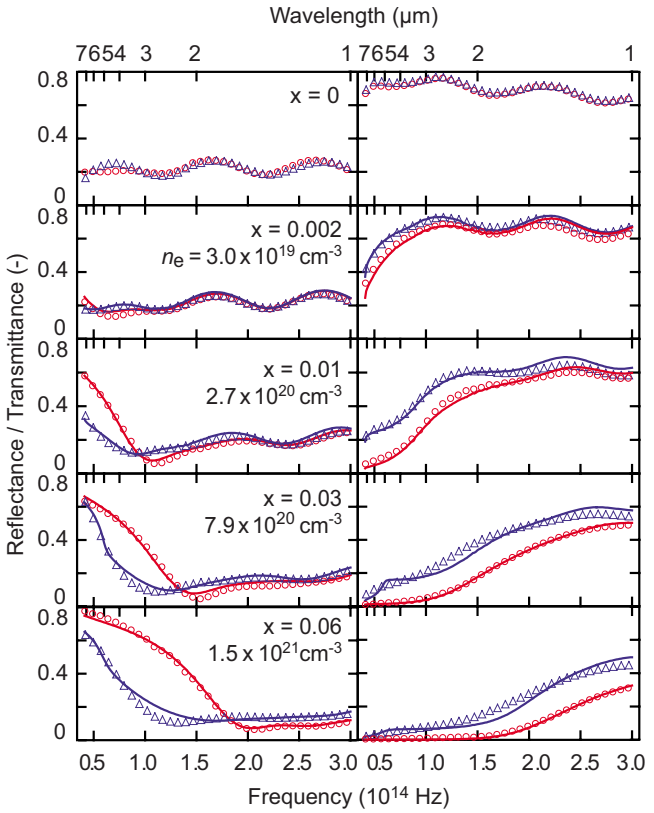


FIG. 3. (Color online) Polarized IR reflection (left panels) and transmission (right panels) spectra of the TNO (102) films with different Nb concentrations ($\mathbf{E}_\parallel$: circle, $\mathbf{E}_\perp$: triangle). The results of least-squares fitting using the Drude model were shown as solid lines.

($x$=0) was highly transparent in the IR region and the spectra were insensitive to the direction of the polarization vectors $\mathbf{E}_\parallel$ and $\mathbf{E}_\perp$. On the other hand, TNO films with $x \geq 0.002$ showed a finite absorption in the IR region, which was strongly dependent on the polarization condition, as seen from shifts of absorption maxima to lower frequency in $\mathbf{E}_\perp$ than in $\mathbf{E}_\parallel$. Because the optical absorption of TNO in the IR region is mainly caused by free carriers,[3,5] the **E** dependence of the spectrum observed here suggests a large anisotropy in $m^*$.

In order to evaluate anisotropic $m^*$ values, we analyzed the PIR spectra using Drude model. On the basis of the crystallographic structure of tetragonal anatase $TiO_2$, the permittivity tensor in crystal coordinate system is expressed by

$$\boldsymbol{\varepsilon}^{\text{crystal}} = \begin{pmatrix} \varepsilon_{\langle 100\rangle}(\omega) & 0 & 0 \\ 0 & \varepsilon_{\langle 100\rangle}(\omega) & 0 \\ 0 & 0 & \varepsilon_{\langle 001\rangle}(\omega) \end{pmatrix}, \quad (1)$$

$$\varepsilon_{\langle hkl\rangle}(\omega) = \varepsilon_{\infty\langle hkl\rangle}\left(1 - \frac{\omega_{p\langle hkl\rangle}^2}{\omega^2 - i\tau^{-1}\omega}\right), \quad (2)$$

$$\omega_{p\langle hkl\rangle}^2 = \frac{n_e q^2}{\varepsilon_{\infty\langle hkl\rangle} \cdot m^*_{\langle hkl\rangle}}, \tag{3}$$

where $\langle hkl\rangle$ represents the principal axis (=$\langle 100\rangle$ or $\langle 001\rangle$), $\varepsilon_{\infty\langle hkl\rangle}$ is the permittivity at the high-frequency limit, $\omega_{p\langle hkl\rangle}$ is the plasma frequency, $\tau$ is the scattering time, $n_e$ is the carrier concentration, and $q$ is the charge of electron.

As mentioned above, our (102)-oriented TNO films consist of two epitaxial domains with 180° different in-plane orientations [domains I and II, see Fig. 2(a)]. These two domains are equivalent under the polarization condition $\mathbf{E}_\parallel$, where the electric field is parallel to the $\langle 100\rangle$ principal axis ($x$ direction). Under the polarization condition $\mathbf{E}_\perp$, on the other hand, the two domains are not equivalent with respect to the electric field. In addition, $\mathbf{E}_\perp$ is not parallel to any of the principal axes of TNO. To treat such a complicated system, we used effective medium approximation (EMA).[11,12] EMA is valid in the present case, because the domain size is much smaller than the wavelength of the incident IR light ($>1$ $\mu$m).

The permittivity tensors of domains I and II in experimental coordinate, $\boldsymbol{\varepsilon}^{\mathrm{I}}$ and $\boldsymbol{\varepsilon}^{\mathrm{II}}$, are described as

$$\boldsymbol{\varepsilon}^{\mathrm{I}} = \begin{pmatrix} \varepsilon_{\langle 100\rangle}(\omega) & 0 & 0 \\ 0 & \varepsilon_{\langle 100\rangle}(\omega)\cos^2\theta + \varepsilon_{\langle 001\rangle}(\omega)\sin^2\theta & [\varepsilon_{\langle 001\rangle}(\omega) - \varepsilon_{\langle 100\rangle}(\omega)]\sin\theta\cos\theta \\ 0 & [\varepsilon_{\langle 001\rangle}(\omega) - \varepsilon_{\langle 100\rangle}(\omega)]\sin\theta\cos\theta & \varepsilon_{\langle 100\rangle}(\omega)\sin^2\theta + \varepsilon_{\langle 001\rangle}(\omega)\cos^2\theta \end{pmatrix},$$

$$\boldsymbol{\varepsilon}^{\mathrm{II}} = \begin{pmatrix} \varepsilon_{\langle 100\rangle}(\omega) & 0 & 0 \\ 0 & \varepsilon_{\langle 100\rangle}(\omega)\cos^2\theta + \varepsilon_{\langle 001\rangle}(\omega)\sin^2\theta & -[\varepsilon_{\langle 001\rangle}(\omega) - \varepsilon_{\langle 100\rangle}(\omega)]\sin\theta\cos\theta \\ 0 & -[\varepsilon_{\langle 001\rangle}(\omega) - \varepsilon_{\langle 100\rangle}(\omega)]\sin\theta\cos\theta & \varepsilon_{\langle 100\rangle}(\omega)\sin^2\theta + \varepsilon_{\langle 001\rangle}(\omega)\cos^2\theta \end{pmatrix}, \tag{4}$$

where $\theta$(=51.5°) is the angle between surface normal ($z$ direction) and the $c$ axis of TNO. For simplicity, we had the following two assumptions. First, the domains are prolate spheroids, of which the long axes are parallel to the surface normal, and the lengths of long and short axes are equivalent to film thickness (~500 nm) and typical domain size (100 nm), respectively. Second, domains I and II have the same volume fractions. Under these conditions, the self-consistent equation for the effective permittivity tensor, $\boldsymbol{\varepsilon}^{\mathrm{eff}}$, is given by[11]

$$[\mathbf{I} - \boldsymbol{\Gamma}(\boldsymbol{\varepsilon}^{\mathrm{I}} - \boldsymbol{\varepsilon}^{\mathrm{eff}})]^{-1}(\boldsymbol{\varepsilon}^{\mathrm{I}} - \boldsymbol{\varepsilon}^{\mathrm{eff}}) + [\mathbf{I} - \boldsymbol{\Gamma}(\boldsymbol{\varepsilon}^{\mathrm{II}} - \boldsymbol{\varepsilon}^{\mathrm{eff}})]^{-1}(\boldsymbol{\varepsilon}^{\mathrm{II}} - \boldsymbol{\varepsilon}^{\mathrm{eff}}) = 0, \tag{5}$$

where $\mathbf{I}$ is the unit tensor and the tensor $\boldsymbol{\Gamma}$ is defined as a surface integral of the Green's function, $G(\mathbf{x}-\mathbf{x}')$, over the surface of a domain, $S'$,

$$\boldsymbol{\Gamma}_{\alpha\beta} = -\oint_{S'} \frac{\partial}{\partial x_\alpha} G(\mathbf{x}-\mathbf{x}') n'_\beta d^2x', \tag{6}$$

where Greek subscripts denote Cartesian components in experimental coordinate system and $\mathbf{n}'$ is a unit normal vector outward from $S'$. Considering the second assumption, the mixture of domains I and II has $C_{2\mathrm{V}}$ (2 mm) symmetry in a scale of the wavelength of probe light, where the $C_2$ axis is parallel to the $z$ axis, and two mirror planes include $x$ or $y$ axis. This symmetry requires $\varepsilon^{\mathrm{eff}}_{\alpha\beta} = -\varepsilon^{\mathrm{eff}}_{\alpha\beta}$, that is, $\boldsymbol{\varepsilon}^{\mathrm{eff}}$ should have a diagonal form. Therefore, the Green's function takes the form

$$G(\mathbf{x}-\mathbf{x}') = \frac{1}{4\pi\sqrt{\varepsilon^{\mathrm{eff}}_{xx}\varepsilon^{\mathrm{eff}}_{yy}\varepsilon^{\mathrm{eff}}_{zz}}} \times \left(\frac{(x-x')^2}{\varepsilon^{\mathrm{eff}}_{xx}} + \frac{(y-y')^2}{\varepsilon^{\mathrm{eff}}_{yy}} + \frac{(z-z')^2}{\varepsilon^{\mathrm{eff}}_{zz}}\right)^{-1/2} \tag{7}$$

Thus, we can deduce the relation between $\boldsymbol{\varepsilon}^{\mathrm{eff}}$ and $m^*$ by numerically solving the self-consistent Eq. (5) using Eqs. (2)–(4), (6), and (7).

PIR reflectance $R(\omega)$ and transmittance $T(\omega)$ spectra under the polarization conditions $\mathbf{E}_\parallel$ and $\mathbf{E}_\perp$ are given as functions of $\varepsilon^{\mathrm{eff}}_{xx}(\omega)$ and $\varepsilon^{\mathrm{eff}}_{yy}(\omega)$, respectively, which are related to $m^*_{\langle 001\rangle}$ and $m^*_{\langle 100\rangle}$ through the above discussion. We obtained these $m^*$ values by least-squares analyses using the above-mentioned $\boldsymbol{\varepsilon}^{\mathrm{eff}}-m^*$ relation, where the multiple reflection interference in the films[13] was taken into account. For carrier concentration $n_e$ and film thickness $d$, we used experimental values determined by Hall and stylus profiler measurements. The $\varepsilon_{\infty\langle hkl\rangle}$ value of TNO was assumed to be the same as that of pure anatase $TiO_2$, i.e., 5.9 for $\mathbf{E}_\parallel$ and 5.8 for $\mathbf{E}_\perp$.[14] We also solve the self-consistent equation assuming different domain sizes, 50 nm and 200 nm, and confirmed that the influence of domain size on $m^*$ is negligibly small.

Figure 3 also includes the results of the curve-fitting (solid lines). The simulated IR spectra reproduce the observed spectra well, which validates the present Drude analysis. The $m^*_{\langle 100\rangle}$ and $m^*_{\langle 001\rangle}$ values obtained for TNO are plotted against $n_e$ in Fig. 4. The $m^*_{\langle 100\rangle}$ at $n_e = 3.0\times10^{19}$ cm$^{-3}$ ($x=0.002$) is approximately 0.2 $m_0$, and it increases up to

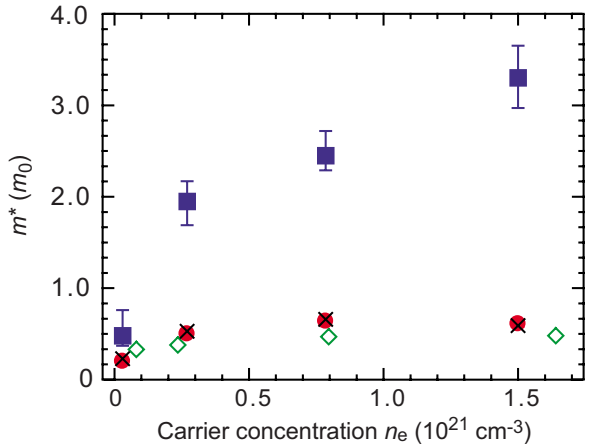


FIG. 4. (Color online) Electron mass $m^*$ of the TNO films along the ⟨100⟩ (circle) and ⟨001⟩ (square) directions as functions of carrier concentration. The error bars denote experimental uncertainty in $m^*$, which originates from light absorption by the substrate, light scattering, and experimental errors in $n_e$. Equation (5) was solved by iterative procedure, and the numerical uncertainty is smaller than the experimental one. The $m^*_{\langle 100\rangle}$ values obtained from (001)-oriented TNO films were plotted for comparison (cross: this study, diamond: Ref. 3).

$\sim 0.6\ m_0$ as $n_e$ increases to $7.9\times10^{20}$ cm$^{-3}$ ($x=0.03$), reflecting the nonparabolicity of the conduction band.[3] These values are in good agreement with the measured values for (001)-oriented TNO films as shown in Fig. 4. In contrast, $m^*_{\langle 001\rangle}$ is 3–6 times larger than $m^*_{\langle 100\rangle}$ for the whole $n_e$ range examined in this study. This implies that TNO is more conductive along the $a$ axis than along the $c$ axis, leading us to the conclusion that control of crystallographic orientation is essential for further improvement in the conductivity of polycrystalline TNO films.

Recent thermoelectric measurements of TNO films reported $m^*_{\mathrm{DOS}}$ to be 0.34 $m_0$ for $n_e=1.1\times10^{19}$ cm$^{-3}$ (Ref. 7) and $\sim 1\ m_0$ for $n_e>1\times10^{20}$ cm$^{-3}$,[6,7] which are considerably larger than $m^*_{\langle 100\rangle}$, 0.3–0.5 $m_0$, as evaluated through optical measurements.[3] Since $m^*_{\mathrm{DOS}}$ is the geometrical average of $m^*$ over all directions ($m^*_{\mathrm{DOS}}=m^{*2/3}_{\langle 100\rangle}\times m^{*1/3}_{\langle 001\rangle}$), the present observed mass anisotropy could explain the difference between $m^*_{\mathrm{DOS}}$ and $m^*_{\langle 100\rangle}$. That is, the $m^*_{\mathrm{DOS}}$ values derived from our $m^*$ data, i.e., $m^*_{\mathrm{DOS}}=m^{*2/3}_{\langle 100\rangle}\times m^{*1/3}_{\langle 001\rangle}=0.3m_0$ for $n_e=3.0\times10^{19}$ cm$^{-3}$ and $0.8-1.1m_0$ for $n_e>0.8\times10^{20}$ cm$^{-3}$, agree well with the experimental values mentioned above.

Table I compares $m^*\|c$ and $m^*\perp c$ of TNO and conventional $s$-electron-based TCOs. The latter show $m^*$ values in the range $0.2-0.3m_0$ with small mass anisotropy, mainly originating from the anisotropic cation-cation distances of host materials. For example, the slightly smaller $m^*_{\langle 001\rangle}$ compared to $m^*_{\langle 100\rangle}$ seen in rutile $SnO_2$ is due to the shorter Sn-Sn distance along the $c$ axis (0.319 nm) as compared to that in the $a$ direction (0.371 nm). In TNO, on the other hand, $m^*$ is highly anisotropic: $m^*_{\langle 100\rangle}$ is comparable to those of other TCOs, but $m^*_{\langle 001\rangle}$ is substantially larger. This indicates that the large electron mass anisotropy in TNO is attributable to the anisotropicity of not only the crystal structure but also Ti $3d$ orbitals.

TABLE I. Electron mass anisotropy of TCO host materials.

| Material | Crystal structure | $m^*\|c(m_0)$ | $m^*\perp c(m_0)$ | Ref. |
|---|---|---|---|---|
| $In_2O_3$ | Bixbyite (cubic) | 0.3 | | 15 |
| ZnO | Wurtzite | — | 0.24 | 16 |
| | (Hexagonal) | 0.31 | 0.33 | 17[a] |
| $SnO_2$ | Rutile (Tetragonal) | 0.23 | 0.30 | 18 |
| $TiO_2$ [b] | Anatase | — | 0.5 | 3 |
| | (Tetragonal) | 2.4 | 0.6 | This study |

[a]Obtained from LCAO calculation.
[b]Determined for $Ti_{0.97}Nb_{0.03}O_2$.

Recently, Kamisaka *et al.*[19] performed first-principles band calculation of TNO ($Ti_{0.9375}Nb_{0.0625}O_2$) based on density-functional theory. They showed that the band structure of TNO is essentially identical to that of undoped anatase $TiO_2$, previously reported by Asahi *et al.*[20] The bottom of the conduction bands is mainly composed of isolated Ti $3d_{xy}$ orbitals, which spread in the $x$-$y$ plane, resulting in larger $m^*_{\langle 001\rangle}$ than $m^*_{\langle 100\rangle}$. From the band dispersions, anisotropic electron masses were evaluated to be $m^*_{\langle 100\rangle}\sim 0.4\ m_0$ and $m^*_{\langle 001\rangle}\sim 4\ m_0$,[19] which are in good agreement with the present experimental results.

In summary, we have determined the $m^*_{\langle 100\rangle}$ and $m^*_{\langle 001\rangle}$ values of TNO by analyzing PIR spectra of (012)-oriented epitaxial films on the basis of an anisotropic Drude model. The $m^*_{\langle 100\rangle}$ values were in the range $0.2-0.6\ m_0$, which is comparable to those of conventional TCOs, while $m^*_{\langle 001\rangle}$ was 3–6 times larger. This large anisotropy is attributable to *both* the anisotropic crystal structure and $d$-orbital-dominated conduction band, which is a unique feature of TNO not found in other conventional TCOs.

We thank K. Itaka and S. Yaginuma of the University of Tokyo and Y. Yukioka of KAST for their kind assistance with PIR measurements. This research was partially supported by MEXT Elements Science and Technology Project.

[1] D. S. Ginley and C. Bright, MRS Bull. **25**, 15 (2000).
[2] Y. Furubayashi, T. Hitosugi, Y. Yamamoto, K. Inaba, G. Kinoda, Y. Hirose, T. Shimada, and T. Hasegawa, Appl. Phys. Lett. **86**, 252101 (2005).
[3] Y. Furubayashi, N. Yamada, Y. Hirose, Y. Yamamoto, M. Otani, T. Hitosugi, T. Shimada, and T. Hasegawa, J. Appl. Phys. **101**, 093705 (2007).
[4] T. Hitosugi, A. Ueda, S. Nakao, N. Yamada, Y. Furubayashi, Y. Hirose, T. Shimada, and T. Hasegawa, Appl. Phys. Lett. **90**, 212106 (2007).

[5] N. Yamada, T. Hitosugi, N. L. H. Hoang, Y. Furubayashi, Y. Hirose, T. Shimada, and T. Hasegawa, Jpn. J. Appl. Phys., Part 1 **46**, 5275 (2007).
[6] D. Kurita, S. Ohta, K. Sugiura, H. Ohta, and K. Koumoto, J. Appl. Phys. **100**, 096105 (2006).
[7] T. Tsuruhama, T. Hitosugi, Y. Furubayashi, N. Yamada, T. Shimada, and T. Hasegawa (unpublished).
[8] Y. Hirose, N. Yamada, S. Nakao, T. Hitosugi, T. Shimada, and T. Hasegawa (unpublished).
[9] R. J. Kennedy and P. A. Stampe, J. Cryst. Growth **252**, 333 (2003).
[10] W. Gao, R. Klie, and E. I. Altman, Thin Solid Films **485**, 115 (2005).
[11] D. Stroud, Phys. Rev. B **12**, 3368 (1975).
[12] T. K. Xia, P. M. Hui, and D. Stroud, J. Appl. Phys. **67**, 2736 (1990).
[13] O. S. Heavens, *Optical Properties of Thin Solid Films* (Dover, New York, 1991), Chap. 5.
[14] N. Hosaka, T. Sekiya, C. Satoko, and S. Kurita, J. Phys. Soc. Jpn. **66**, 877 (1997).
[15] Z. M. Jarzebski, Phys. Status Solidi A **71**, 13 (1982).
[16] W. S. Baer, Phys. Rev. **154**, 785 (1967).
[17] M.-Z. Huang and W. Y. Ching, J. Phys. Chem. Solids **46**, 977 (1985).
[18] K. J. Button, D. G. Fonstad, and W. Dreybradt, Phys. Rev. B **4**, 4539 (1971).
[19] H. Kamisaka, T. Hitosugi, T. Suenaga, T. Hasegawa, and K. Yamashita (unpublished).
[20] R. Asahi, Y. Taga, W. Mannstadt, and A. J. Freeman, Phys. Rev. B **61**, 7459 (2000).